図2 パーキンソン病の二大病因仮説に基づく神経変性経路（文献[11]より改変引用）

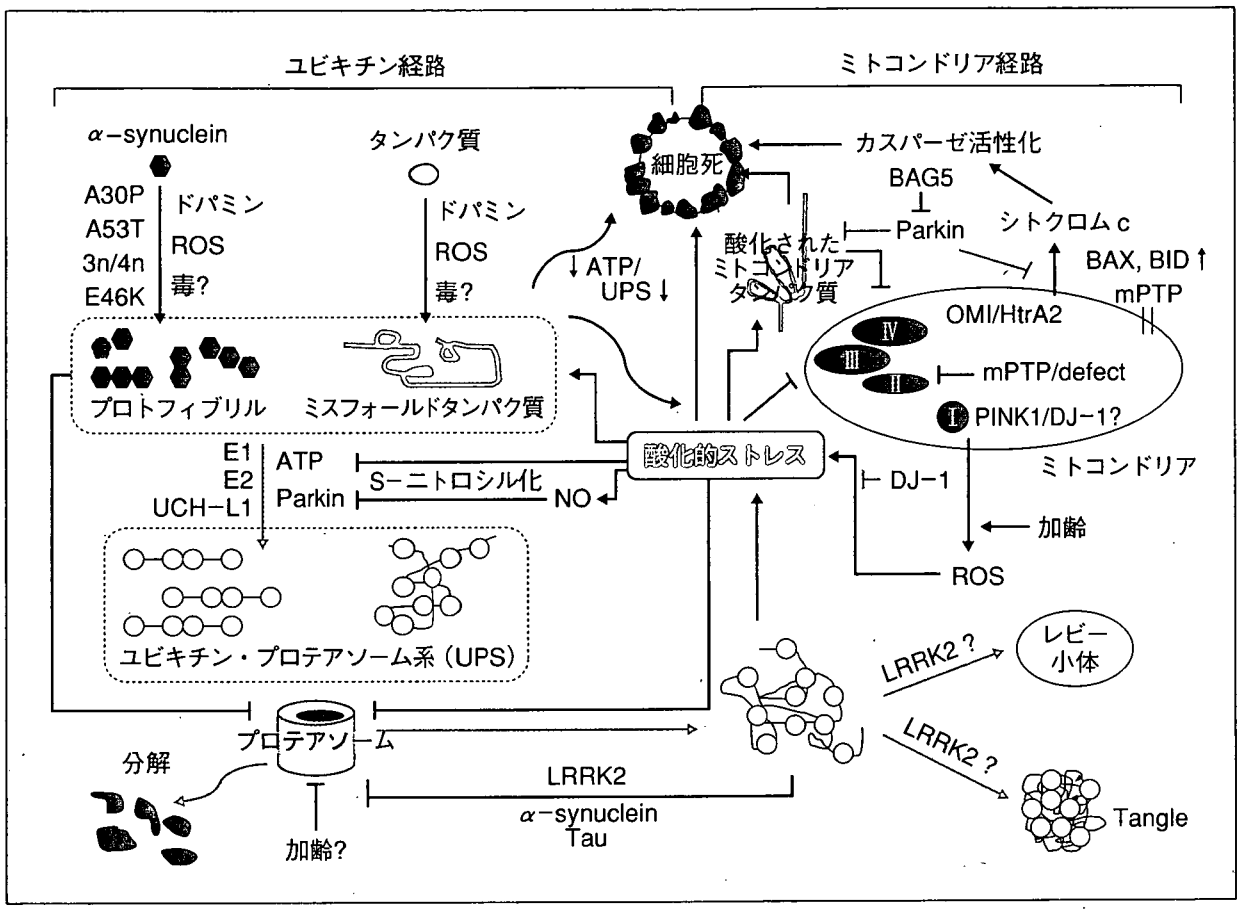

略語：巻末の「今月の略語」参照

キチン・プロテアソーム系の障害が病因仮説として浮上してきたことから，プロテアソーム阻害剤のラットへの全身投与によるパーキンソン病モデル作製の試みが行われた．最初の報告では，症状・病理所見ともパーキンソン病に類似した病的変化が起こるとされ注目された．しかし再現性に問題があることが複数の研究室から指摘され，現在はこの方法によるモデル作製は困難と考えられている[16]．

二大仮説
―異常タンパク質蓄積とミトコンドリア機能不全―

これまでの研究の流れをまとめると，α-synuclein，Parkin の研究から導かれた「異常タンパク質の蓄積」と，PINK1，DJ-1 の研究や患者検体，毒物の研究から注目されてきた「ミトコンドリア機能障害」が，パーキンソン病発症の二大仮説として有力である．この2つの仮説はお互いに矛盾するものではなく，密接に絡み合っているものと考えられる（図2）[11]．現段階での実験的証拠から，2つの考え方を結びつける最も重要なキーワードは酸化的ストレスである．ミトコンドリアは酸素呼吸をすると同時に酸化的ストレスを恒常的に産生している装置であるが，活性酸素はタンパク質を酸化してミスフォールド化させる，Parkin やプロテアソームサブユニットを酸化修飾して不活性化させる，などの作用で異常タンパク質蓄積を促進すると考えられる．一方，異常タンパク質処理に当たって ATP 依存的プロテアーゼである 26S プロテアソームが動員されると，ATP 産生亢進の必要性からミトコンドリアに負荷がかかる

ことも想像される．さらに前述の Parkin と PINK1 の機能関連の解明は，ユビキチン・プロテアソーム系とミトコンドリアの関係に新たな視点を与えることになるであろう．

おわりに
―階層を越えたパーキンソン病の統合的理解に向けて―

以上，パーキンソン病発症メカニズムに関する分子・細胞レベルでの研究の現状と今後の見通しについて述べてきた．しかし，パーキンソン病が細胞の病気であるとともにシステムの病気であるという観点を忘れると，疾患の本質を見失うおそれがある．もし冒頭に述べた Braak の仮説が正しければ，ドパミン神経変性が始まる前にパーキンソン病は発症していることになり，その時期に治療することができれば運動障害の発症を抑えることができるかもしれない．そういう点から，ドパミン神経細胞死のみに焦点を絞ったこれまでの研究からのパラダイムシフトが求められていると言えよう．例えば，Braak の仮説や心臓交感神経の障害に示されるような「パーキンソン病は全身病である」というシステムとしての疾患概念の妥当性を分子・細胞レベルで検証することが，階層性を越えてパーキンソン病を統合的に理解する端緒となるであろうし，これからの研究が挑戦すべき大きな課題であると思われる．

文　献

1) Braak H, et al: Stages in the development of Parkinson's disease-related pathology. Cell Tissue Res 318: 121–134, 2004.
2) Chaudhuri K R, et al: Non-motor symptoms of Parkinson's disease: diagnosis and management. Lancet Neurol 5: 235–245, 2006.
3) Orimo S, et al: Cardiac sympathetic denervation precedes neuronal loss in the sympathetic ganglia in Lewy body disease. Acta Neuropathol (Berl) 109: 583–588, 2005.
4) Hardy J, et al: Genetics of Parkinson's disease and parkinsonism. Ann Neurol 60: 389–398, 2006.
5) Baba M, et al: Aggregation of alpha-synuclein in Lewy bodies of sporadic Parkinson's disease and dementia with Lewy bodies. Am J Pathol 152: 879–884, 1998.
6) Mizuta I, et al: Multiple candidate gene analysis identifies alpha-synuclein as a susceptibility gene for sporadic Parkinson's disease. Hum Mol Genet 15: 1151–1158, 2006.
7) Volles M J, et al: Zeroing in on the pathogenic form of alpha-synuclein and its mechanism of neurotoxicity in Parkinson's disease. Biochemistry 42: 7871–7878, 2003.
8) Tanaka Y, et al: Inducible expression of mutant alpha-synuclein decreases proteasome activity and increases sensitivity to mitochondria-dependent apoptosis. Hum Mol Genet 10: 919–926, 2001.
9) Imai Y, et al: How do Parkin mutations result in neurodegeneration? Curr Opin Neurobiol 14: 384–389, 2004.
10) Matsuda N, et al: Diverse effects of pathogenic mutations of Parkin that catalyze multiple monoubiquitylation *in vitro*. J Biol Chem 281: 3204–3209, 2006.
11) Abou-Sleiman P M, et al: Expanding insights of mitochondrial dysfunction in Parkinson's disease. Nat Rev Neurosci 7: 207–219, 2006.
12) Tan J M, et al: Parkin blushed by PINK1. Neuron 50: 527–529, 2006.
13) Suzuki Y, et al: A serine protease, HtrA2, is released from the mitochondria and interacts with XIAP, inducing cell death. Mol Cell 8: 613–621, 2001.
14) Ramirez A, et al: Hereditary parkinsonism with dementia is caused by mutations in ATP13A2, encoding a lysosomal type 5 P-type ATPase. Nat Genet 38: 1184–1191, 2006.
15) Schapira A H: Etiology of Parkinson's disease. Neurology 66: S10–23, 2006.
16) Beal F, et al: The proteasomal inhibition model of Parkinson's disease: "Boon or bust"? Ann

Neurol 60: 158–161, 2006.

Approaches to the Elucidation of the Pathogenetic Mechanisms Underlying Parkinson's Disease

Ryosuke Takahashi
Department of Neurology, Kyoto University Graduate School of Medicine

nature neuroscience

Astrocytes as determinants of disease progression in inherited amyotrophic lateral sclerosis

Koji Yamanaka[1,2], Seung Joo Chun[1], Severine Boillee[1], Noriko Fujimori-Tonou[2], Hirofumi Yamashita[2], David H Gutmann[3], Ryosuke Takahashi[4], Hidemi Misawa[5] & Don W Cleveland[1]

Dominant mutations in superoxide dismutase cause amyotrophic lateral sclerosis (ALS), an adult-onset neurodegenerative disease that is characterized by the loss of motor neurons. Using mice carrying a deletable mutant gene, diminished mutant expression in astrocytes did not affect onset, but delayed microglial activation and sharply slowed later disease progression. These findings demonstrate that mutant astrocytes are viable targets for therapies for slowing the progression of non–cell autonomous killing of motor neurons in ALS.

ALS is an adult-onset neurodegenerative disease, characterized by a progressive and fatal loss of motor neurons. Dominant mutations in the gene for superoxide dismutase (*SOD1*) are the most frequent cause of inherited ALS. Ubiquitous expression of mutant *SOD1* in rodents leads to progressive, selective motor neuron degeneration as a result of acquired toxic properties. The exact mechanism responsible for motor neuron degeneration in ALS, however, is not known[1,2]. Mutant damage in the vulnerable motor neurons is a key determinant of disease onset[3], whereas accumulating evidence supports an active role of non-neuronal cells in motor neuron degeneration[3–7]. Evidence with selective gene excision[3] or bone-marrow grafting[5] has demonstrated that mutant SOD1-derived damage in microglia accelerates later disease progression. Despite the importance of astrocyte function, the role of mutant action in astrocytes in disease has not been tested *in vivo*.

To examine whether mutant SOD1 damage in astrocytes contributes to disease, *loxSOD1*^{G37R} mice[3], carrying a mutant *SOD1* gene that can be deleted by the action of the Cre recombinase, were mated with *GFAP-Cre* mice (**Fig. 1** and **Supplementary Fig. 1** online), which express both Cre recombinase and β-galactosidase (*LacZ*) under the control of the human GFAP promoter[8]. Mice from these matings that carry the *GFAP-Cre* transgene are denoted as Cre$^+$, whereas mice without it are referred to as Cre$^-$. To determine the cell-type specificity of Cre expression in the spinal cord, *GFAP-Cre* mice were mated to Rosa26 mice, which ubiquitously express a *LacZ* gene that encodes functional β-galactosidase only after Cre-mediated recombination. Although this *GFAP-Cre* transgene is expressed in a subset of neurons in the cerebellum and hippocampus during embryogenesis[9], measurement of β-galactosidase activity (by deposition of a blue reaction product after addition of the X-gal substrate) demonstrated that Cre expression and Cre-mediated recombination was restricted in the spinal cord to GFAP-reactive astrocytes (**Fig. 1a,b**). The efficiency of mutant gene excision in cultured astrocytes from newborn *loxSOD1*^{G37R}*/GFAP-Cre*$^+$ mice was ~76% (**Fig. 1d,e**), determined by quantitative PCR for human SOD1 transgene number (**Fig. 1d**) and immunoblotting for mutant SOD1 levels (**Fig. 1e**). We observed neither detectable Cre activity nor mutant gene excision in microglia (**Fig. 1c** and **Supplementary Fig. 2** online).

A simple, objective measure of disease onset and early disease was applied by initiation of weight loss, itself reflecting denervation-induced muscle atrophy. Reduction of SOD1^{G37R} in astrocytes did not slow disease onset nor early disease (GFAP-Cre$^+$, 341.6 ± 48.9 d; GFAP-Cre$^-$, 337.0 ± 35.8 d; **Fig. 1f,h**). However, late disease progression (from early disease to end stage) was sharply delayed, providing a mean extension of survival by 48 d (Cre$^+$, 87.4 d; Cre$^-$, 39.5 d; **Fig. 1j**). Progression from onset to early disease was more modestly slowed by 14 d (Cre$^+$, 99.3 d; Cre$^-$, 85.2 d; **Fig. 1i**). Overall survival was extended by 60 d (Cre$^+$, 436.5 ± 38.8 d; Cre$^-$, 376.5 ± 26.9 d; **Fig. 1g**). This contrasts with delayed disease onset from diminished mutant synthesis solely within motor neurons (with a *VAChT-Cre* transgene carrying the motor neuron–specific vesicular acetylcholine transporter promoter) without affecting disease progression (**Supplementary Results**, **Supplementary Methods** and **Supplementary Fig. 3** online), just as reported previously with an *Isl1* (*Islet1*)*-Cre* transgene that is expressed in motor neurons and some peripheral tissues[3].

Astrocytic and microglial cell activation is a well-accepted feature of SOD1 mutant–mediated ALS[1,2]. An elevated proportion of GFAP-positive astrocytes appeared before disease onset (**Fig. 2a**) in *loxSOD1*^{G37R} mice. This astrogliosis was progressive, readily apparent by onset (**Fig. 2b**) and more prominent during disease progression (**Fig. 2c**). Despite substantial mutant reduction, astrogliosis was not, however, different in comparing disease-matched *loxSOD1*^{G37R}*/GFAP-Cre*$^+$ mice (**Fig. 2d,e**) and *loxSOD1*^{G37R}*/GFAP-Cre*$^-$ mice (**Fig. 2b,c**).

Microglial activation occurred at earliest disease onset in *Cre*$^-$ mice (**Fig. 2g**) and was progressively more prominent during disease progression (**Fig. 2h**). Microglial activation was, however, substantially delayed from onset through early disease in the *GFAP-Cre*$^+$ mice when mutant SOD1 levels were reduced only in astrocytes (**Fig. 2i,j**). By exploiting the presence of β-galactosidase to mark astrocytes with diminished SOD1 mutant synthesis, examination of sections throughout lumbar spinal cords of symptomatic *loxSOD1*^{G37R}*/GFAP-Cre*$^+$ mice

[1]Ludwig Institute for Cancer Research and Department of Medicine and Neuroscience, University of California at San Diego, 9500 Gilman Drive, La Jolla, California 92093-0670, USA. [2]Yamanaka Research Unit, RIKEN Brain Science Institute, 2-1 Hirosawa, Wako, Saitama 351-0198, Japan. [3]Department of Neurology, Washington University School of Medicine, 660 South Euclid Avenue, St. Louis, Missouri 63110, USA. [4]Department of Neurology, Graduate School of Medicine, Kyoto University, 54 Shogoin Kawahara-cho, Sakyo-ku, Kyoto 606-8507, Japan. [5]Department of Pharmacology, Kyoritsu University of Pharmacy, 1-5-30 Shibakoen, Minato-ku, Tokyo 105-8512, Japan. Correspondence should be addressed to D.W.C. (dcleveland@ucsd.edu) or K.Y. (kyamanaka@brain.riken.jp).

Received 26 November 2007; accepted 7 January 2008; published online 3 February 2008; doi:10.1038/nn2047

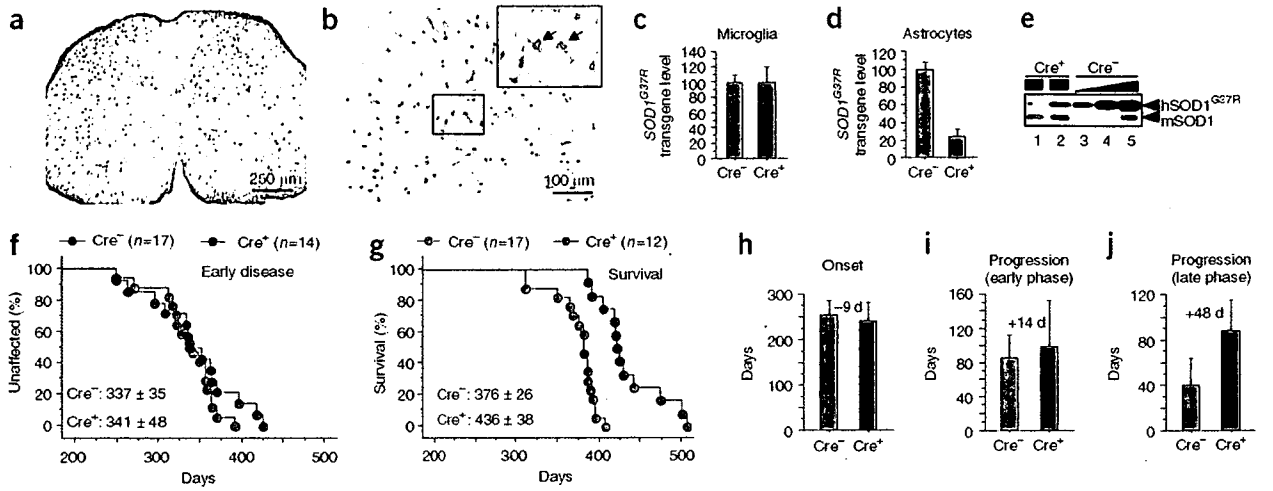

Figure 1 Selective Cre-mediated gene excision shows that mutant SOD1 action in astrocytes is a primary determinant of late disease progression. (**a**,**b**) β-galactosidase (β-gal) activity in astrocytes in whole (**a**) or in the anterior horn region (**b**) of the lumbar spinal cord section of *GFAP-Cre*/Rosa26 reporter mice visualized with X-gal and immunostaining with GFAP antibody. Inset, magnified image of the boxed area in **b**. Arrows indicate β-gal/GFAP-Cre–expressing astrocytes. (**c**,**d**) *loxSOD1*^{G37R} transgene levels ($n = 3$ for each group) in primary microglia (**c**) or astrocytes (**d**) from *loxSOD1*^{G37R}/*GFAP-Cre*$^{+}$ and *loxSOD1*^{G37R} mice using real-time PCR. (**e**) We determined SOD1^{G37R} and mouse SOD1 levels by immunoblotting extracts from isolated primary astrocytes of *loxSOD1*^{G37R}/*GFAP-Cre*$^{+}$ (lanes 1, 2) and a dilution series of a comparable extract from LoxSOD1^{G37R} astrocytes representing 25%, 50% and 100% of the protein amounts loaded in lanes 1 and 2 (lanes 3–5). (**f**,**g**) Ages at which early disease phase (to 10% weight loss, $P = 0.76$; **f**) or end-stage disease ($P < 0.0001$; **g**) were reached for *loxSOD1*^{G37R}/*GFAP-Cre*$^{+}$ mice (red) and *loxSOD1*^{G37R} littermates (blue). Mean ages ± s.d. are provided. (**h**–**j**) Mean onset ($P = 0.47$) (**h**), mean duration of early disease (from onset to 10% weight loss, $P = 0.35$; **i**) and a late disease (from 10% weight loss to end stage, $P < 0.0001$; **j**) for *loxSOD1*^{G37R}/*GFAP-Cre*$^{+}$ (red) and *loxSOD1*^{G37R} littermates (blue). At each time point, *P* value was determined by unpaired *t*-test. Error bars denote s.d.

revealed an inverse relationship (**Fig. 3a–g**) between the number of astrocytes with reduced mutant SOD1 (*Cre*$^{+}$) and activated microglia (correlation coefficient, $r = -0.868$, $P < 0.001$), despite comparable astrocytic activation. Thus, microglial activation was most prominent in areas with the highest mutant SOD1–expressing astrocyte concentration.

Elevated production of nitric oxide by upregulated inducible nitric oxide synthase (iNOS) has been reported in mutant SOD1 mice[10], although deletion of the iNOS gene has modest[11] or no[12] effect on SOD1-mediated disease. It is not known in which glial cells this nitric oxide is produced in *in vivo* models of ALS, although both microglia and astrocytes have an ability to produce it when stimulated *in vitro*[13]. Triple staining of lumbar spinal cord sections with iNOS, Mac2 and GFAP antibodies (**Fig. 3h–r**) revealed that almost all iNOS-positive cells were Mac2-positive microglia (**Fig. 3n–r** and **Supplementary Fig. 4** online), indicating that activated microglia are the primary cell type producing nitric oxide in this SOD1 mouse model. Diminishing mutant synthesis in astrocytes inhibited iNOS induction in disease-matched, symptomatic SOD1 mice (**Fig. 3h,k**), consistent with substantial inhibition of microglial activation (**Fig. 3i,l**).

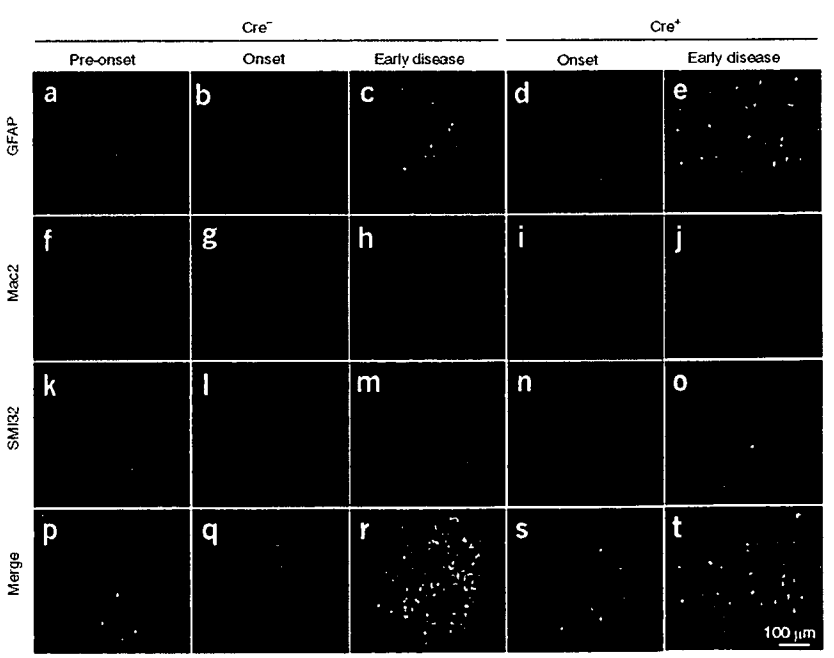

Figure 2 Selective downregulation of mutant SOD1 in astrocytes significantly inhibits microglial activation. (**a**–**t**) GFAP-positive astrocytes (**a**–**e**), Mac2-positive activated microglia (**f**–**j**) and motor neurons identified with the neurofilament antibody SMI-32 (**k**–**o**) in the lumbar spinal cord of a *loxSOD1*^{G37R} mouse before disease onset (**a**,**f**,**k**,**p**), at disease onset (**b**,**g**,**l**,**q**) or during early disease (**c**,**h**,**m**,**r**), together with *loxSOD1*^{G37R}/*GFAP-Cre*$^{+}$ mice at disease onset (**d**,**i**,**n**,**s**) or during early disease (**e**,**j**,**o**,**t**). Merged images are shown in **p**–**t**.

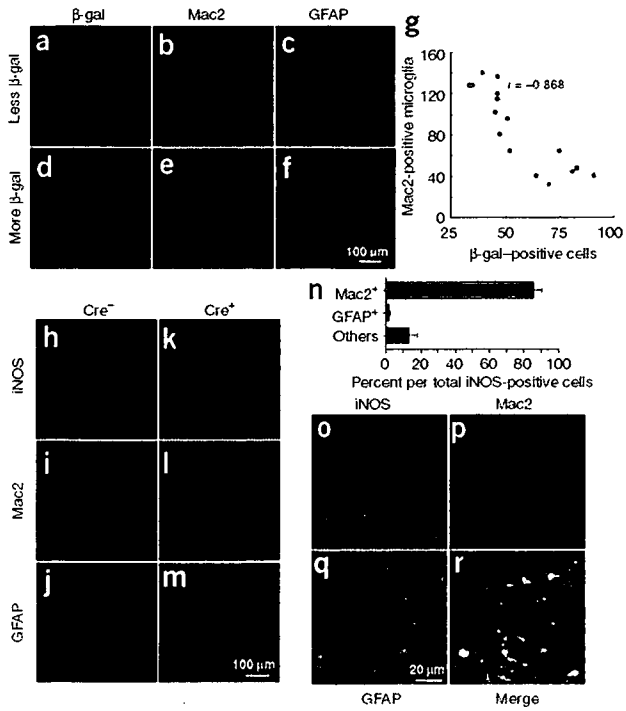

Figure 3 Mutant-expressing astrocytes enhance microglial activation and induction of iNOS. (**a–f**) Images of β-galactosidase (**a,d**), Mac2 (**b,e**) and GFAP (**c,f**) staining from a left (**a–c**) and right (**d–f**) lumbar spinal cord section from a 12-month-old *loxSOD1*^{G37R}*/GFAP-Cre*$^{+}$ mouse. *GFAP-Cre*$^{+}$ astrocytes are marked by β-galactosidase (**a,d**). (**g**) Inverted correlation between the number of Cre-positive astrocytes and Mac2-positive microglia in *loxSOD1*^{G37R}*/GFAP-Cre*$^{+}$ mice lumbar spinal cord sections (correlation coefficient, $r = -0.868$, $P < 0.001$). (**h–m**) Lumbar spinal cord sections from *loxSOD1*^{G37R} (**h–j**) and *loxSOD1*^{G37R}*/GFAP-Cre*$^{+}$ (**k–m**) mice at the early disease stage immunostained with antibodies to iNOS (**h,k**), Mac2 (**i,l**), and GFAP (**j,m**). (**n**) Quantification of iNOS-positive cells in the anterior horn from lumbar spinal cord of symptomatic *loxSOD1*^{G37R} mice. We plotted the averaged percent of iNOS^{+}/Mac2^{+} (red), iNOS^{+}/GFAP^{+} (blue) and iNOS^{+}/other cell type (black) per total iNOS^{+} cells. (**o–r**) Magnified images of anterior horn from lumbar spinal cord of symptomatic *loxSOD1*^{G37R} mice stained with iNOS (**o**), Mac2 (**p**) and GFAP (**q**). Merged image illustrates that iNOS-positive cells are Mac2-positive microglia (**r**).

A role for astrocytes in inherited ALS has been previously considered in several contexts. Mutant-expressing astrocytes produce and release one or more as yet uncharacterized components that can accelerate motor neuron death *in vitro*[6,7]. Focal loss of the astrocytic EAAT2 glutamate transporter in affected regions[14] (**Supplementary Fig. 5** online) and the failure of normal glutamate uptake of *SOD1*^{G93A} astrocytes *in vitro*[15] support glutamate-dependent excitotoxicity as a component of disease. Nevertheless, diminished mutant SOD1 synthesis in most astrocytes did not affect disease-dependent loss of EAAT2 from those astrocytes (**Supplementary Fig. 5**), indicating that a reduction in glutamate transport reflects non–cell autonomous damage to astrocytes, in part, from mutant SOD1 synthesized by other cells. Our use of selective gene excision has now demonstrated that mutant SOD1 damage in both microglia[3] and astrocytes (**Fig. 1g–j**) accelerates later disease progression without affecting the initiation of motor neuron degeneration and phenotypic disease onset. Discovery that damage in astrocytes determines the timing of microglial activation and infiltration provides further evidence that, beyond any direct effect of mutant astrocytes on motor neurons, such astrocytes amplify an inflammatory response from microglia (including enhanced production of nitric oxide and possibly of toxic cytokines), leading to further damage to the motor neurons and accelerated disease progression through a non–cell autonomous mechanism (**Supplementary Fig. 6** online). These findings validate therapies, including astrocytic stem cell–replacement approaches, that aim to slow disease progression in ALS by supplementing healthy astrocytes or modulating toxicity in astrocytes to control an inflammatory response of microglia.

Note: Supplementary information is available on the Nature Neuroscience website.

ACKNOWLEDGMENTS

This work was supported by a US National Institutes of Health grant (NS 27036) and a grant from the Packard ALS Center at Johns Hopkins (D.W.C.), as well as a Muscular Dystrophy Association developmental grant, the Uehara Memorial Foundation, the Nakabayashi Trust for ALS Research and a grant-in-aid for Scientific Research (19591021) and on Priority Area (19044048) from the Ministry of Education, Culture, Sports, Science and Technology of Japan (K.Y.). Salary support for D.W.C is provided by the Ludwig Institute for Cancer Research. S.B. is a recipient of a Fondation pour la Recherche Medical fellowship, an Institut National de la santé et de la Recherché Medicale fellowship and a Muscular Dystrophy Association developmental grant.

AUTHOR CONTRIBUTIONS

K.Y., S.J.C., S.B., N.F.-T. and H.Y. conducted the experiments. D.H.G., R.T. and H.M. provided essential experimental tools and advice. K.Y., S.B., and D.W.C. were responsible for the overall design of the project, analyses of the results and writing the manuscript.

Published online at http://www.nature.com/natureneuroscience
Reprints and permissions information is available online at http://npg.nature.com/reprintsandpermissions

1. Pasinelli, P. & Brown, R.H. *Nat. Rev. Neurosci.* **7**, 710–723 (2006).
2. Boillee, S., Vande Velde, C. & Cleveland, D.W. *Neuron* **52**, 39–59 (2006).
3. Boillee, S. *et al. Science* **312**, 1389–1392 (2006).
4. Clement, A.M. *et al. Science* **302**, 113–117 (2003).
5. Beers, D.R. *et al. Proc. Natl. Acad. Sci. USA* **103**, 16021–16026 (2006).
6. Di Giorgio, F.P., Carrasco, M.A., Siao, M.C., Maniatis, T. & Eggan, K. *Nat. Neurosci.* **10**, 608–614 (2007).
7. Nagai, M. *et al. Nat. Neurosci.* **10**, 615–622 (2007).
8. Bajenaru, M.L. *et al. Mol. Cell. Biol.* **22**, 5100–5113 (2002).
9. Fraser, M.M. *et al. Cancer Res.* **64**, 7773–7779 (2004).
10. Almer, G., Vukosavic, S., Romero, N. & Przedborski, S. *J. Neurochem.* **72**, 2415–2425 (1999).
11. Martin, L.J. *et al. J. Comp. Neurol.* **500**, 20–46 (2007).
12. Son, M., Fathallah-Shaykh, H.M. & Elliott, J.L. *Ann. Neurol.* **50**, 273 (2001).
13. Barbeito, L.H. *et al. Brain Res. Brain Res. Rev.* **47**, 263–274 (2004).
14. Howland, D.S. *et al. Proc. Natl. Acad. Sci. USA* **99**, 1604–1609 (2002).
15. Vermeiren, C. *et al. J. Neurochem.* **96**, 719–731 (2006).

Rines/RNF180, a novel RING finger gene-encoded product, is a membrane-bound ubiquitin ligase

Miyuki Ogawa[1,2], Kiyomi Mizugishi[3], Akira Ishiguro[1], Yoshio Koyabu[3], Yuzuru Imai[4], Ryosuke Takahashi[4], Katsuhiko Mikoshiba[2,3] and Jun Aruga[1,*]

[1]*Laboratory for Comparative Neurogenesis, RIKEN Brain Science Institute, Wako-shi, Saitama 351-0198, Japan*
[2]*Division of Molecular Neurobiology, Department of Basic Medical Science, Institute of Medical Science, University of Tokyo, Minato-ku, Tokyo 108-8639, Japan*
[3]*Laboratory for Developmental Neurobiology, RIKEN Brain Science Institute, Wako-shi, Saitama 351-0198, Japan*
[4]*Laboratory for Motor System Neurodegeneration, RIKEN Brain Science Institute, Wako-shi, Saitama 351-0198, Japan*

We identified and characterized a novel RING finger gene, *Rines/RNF180*, which is well conserved among vertebrates. Putative *Rines* gene product (Rines) contains a RING finger domain, a basic coiled-coil domain, a novel conserved domain (DSPRC) and a C-terminal hydrophobic region that is predicted to be a transmembrane domain. N-terminally epitope tagged-Rines (Nt-Rines) was detected in the endoplasmic reticulum membrane/nuclear envelope in cultured mammalian cells. Nt-Rines was not extracted by high salt or alkaline buffers and was degraded in intact endoplasmic reticulum treated with proteinase K, indicating that Nt-Rines is an integral membrane protein with most of its N-terminal regions in the cytoplasm. *Rines* was expressed in brain, kidney, testis and uterus of adult mice, and in developing lens and brain, particularly in the ventricular layer of the cerebral cortex at embryonic stages. In cultured cells, Nt-Rines can bind another protein and promoted its degradation. The degradation was inhibited by proteasomal inhibitors. In addition, Nt-Rines itself was heavily ubiquitinated and degraded by proteasome. The involvement of Rines in the ubiquitin–proteasome pathway was further supported by its binding to the UbcH6 ubiquitin-conjugating enzyme and by its trans-ubiquitination enhancing activities. These results suggest that Rines is a membrane-bound E3 ubiquitin ligase.

Introduction

Protein degradation by the proteasome pathway plays a vital role in controlling the level of proteins involved in diverse cellular processes, including differentiation, proliferation and apoptosis (Hershko & Ciechanover 1998; Pickart 2001). In the ubiquitin–proteasome pathway, substrates are marked by covalent linkage to ubiquitin for degradation. The ubiquitinated proteins are then recognized and degraded by the 26S proteasome. Ubiquitination involves highly specific enzyme cascades such as E1 ubiquitin-activating enzyme, E2 ubiquitin-conjugating enzyme and E3 ubiquitin-protein ligase (Hershko & Ciechanover 1998; Pickart 2001). Among them, E3 ubiquitin ligase plays a key role in determining the specificity and timing of the ubiquitination of substrates and subsequent protein degradation. Many E3 ubiquitin ligases contain a RING finger domain as a binding domain for E2 enzymes (Joazeiro & Weissman 2000; Pickart 2001).

A novel RING finger motif-containing gene, *Rines*, was found in a screening for binding partner of Zic2, which belongs to the Zic family nuclear zinc finger proteins (Aruga *et al.* 1996; Nagai *et al.* 2000; Mizugishi *et al.* 2004). Because a putative *Rines* gene product (Rines) does not show any close similarities to previously known proteins, its basic molecular properties were investigated using Zic2 as a tool protein. We characterized the structure, subcellular localization, topology and molecular functions of Rines, together with the expression profiles of *Rines* in developing and adult mice. We found that *Rines* was expressed in developing and mature brain and in other organs. Rines possessed a RING finger domain that is necessary for ubiquitin ligase activity and a novel domain, and was an integral membrane protein located

Communicated by: Hiroshi Hamada
**Correspondence*: Email: jaruga@brain.riken.jp

DOI: 10.1111/j.1365-2443.2008.01169.x

mainly on the cytoplasmic side of the endoplasmic reticulum. Molecular function analyses revealed proteasomal degradation-enhancing, degradation target-binding and E2 enzyme-binding activities. Our results indicated Rines to be a novel proteasomal degradation mediator.

Results

Structural features of the Rines

In a yeast-two hybrid screening of an E10.5 mouse embryonic cDNA library using an entire N-terminal half of the mouse Zic2 protein (1–255) as a bait (Mizugishi *et al.* 2004), we isolated a clone that encodes part of a novel RING finger motif, the gene of which we named *Rines* (An abbreviation of *RING finger protein in neural stem cells*).

Nucleotide sequencing of the *Rines* cDNA revealed that the putative open reading frame (ORF) contains 1773 nucleotides (591 amino acids, accession: AAH46775, also named as *RNF180* in a cDNA collection project (Strausberg *et al.* 2002)). The predicted *Rines* gene product (Rines) is a 65 kDa protein containing a RING finger domain (Fig. 1A–C). The RING finger domain is a cysteine/histidine rich (C3HC4), Zn^{2+} binding domain that has been found in a number of eukaryotic proteins and considered to be chemical catalysts and molecular scaffolds that bring other proteins together (Borden 2000). Emerging evidence indicates that RING finger motif may have ubiquitin ligase activity and function in protein ubiquitination (Joazeiro & Weissman 2000; Pickart 2001). In its C-terminal end, there is a hydrophobic region, which is predicted to be a transmembrane segment by computer programs (SOSUI, Hirokawa *et al.* 1998, PHDHTM, Rost *et al.* 1996).

A homology search against BLAST/NCBI database revealed the presence of the mouse Rines homologues in human, chick, and zebrafish (Fig. 1B). The RING finger domain was strongly conserved among the Rines homologues. In addition, there were three conserved domains in an N-terminal region, an N-terminal flanking of the RING finger domain and a C-terminal portion. A homology search revealed that the N-terminally located conserved domains had a significant homology to proteins including dual specificity protein phosphatases, rat GKAP (Munoz-Alonso *et al.* 2000) and yeast Yvh1 (Giaever *et al.* 2002) (Fig. 1D). This conserved domain (named here as DSPRC, dual specificity phosphatase–Rines-conserved) is consisted of about 50 amino acids residues where four cysteine residues are absolutely conserved, and is also detected in insect and plant proteins. However, functional significance of DSPRC is not clear at this point. The second conserved region contained a cluster of basic residues. In addition, a computer program (ISREC-Coil server, <http://www.isrec.ish-sib.ch/cgi-bin/COILS-from-paser>) predicted the presence of a coiled-coil structure, which is known to mediate protein-to-protein interaction. The coiled-coil domain was also predicted in all the vertebrate Rines homologues. In the current protein database, we did not find any other proteins with a domain organization similar to that of Rines (Fig. 1A), suggesting that Rines is a unique protein.

Rines is a membrane-anchored protein

We first characterized Rines in terms of its subcellular localization. When N-terminally Flag epitope-tagged Rines (Flag-Rines) was produced in cells, it was detected as reticular staining in the cytoplasmic region (Fig. 2A). The staining greatly overlapped that of Calnexin, an endoplasmic reticulum (ER)-anchored integral membrane protein, suggesting ER membrane/nuclear envelope localization of Rines. Similarly to Calnexin, Flag-Rines was extracted from membrane fractions only in buffers containing detergents, but not in the presence of urea, salt alone or an alkaline buffer (Fig. 2B). In contrast, Calreticulin, a peripheral membrane protein of the ER, was extracted from the membrane fractions in an alkaline buffer (Fig. 2B). Peripheral membrane proteins can be separated from integral membrane proteins by extraction with 0.1 M Na_2CO_3 (Fujiki *et al.* 1982). These results indicate that Flag-Rines is an integral membrane protein, in agreement with the presence of the predicted transmembrane region. When the crude membrane fraction was treated with proteinase K in the absence of detergent, N-terminally Myc-tagged Rines was digested similarly to the ER membrane protein TRAPα, whereas BiP, an intraluminal ER protein, was mostly not (Fig. 2C). This result indicates that most of the N-terminus of Myc-Rines is located in the cytoplasm.

Expression pattern of *Rines*

The expression profile of *Rines* in mice was first examined by Northern blot analysis (Fig. 3A,B). In adult mice, the *Rines* mRNA was most strongly detected in brain, moderately in kidney, testis and uterus and weakly in lung and thymus (Fig. 3A). In the course of development, significant expression was detected from E10.5, the mRNA level was gradually increased, peaked around E13.5 and then gradually decreased (Fig. 3B). These results suggest that *Rines*, in principle, could play a role in the later gestational development.

To determine the spatial expression pattern of *Rines*, we performed a series of *in situ* hybridization histochemical

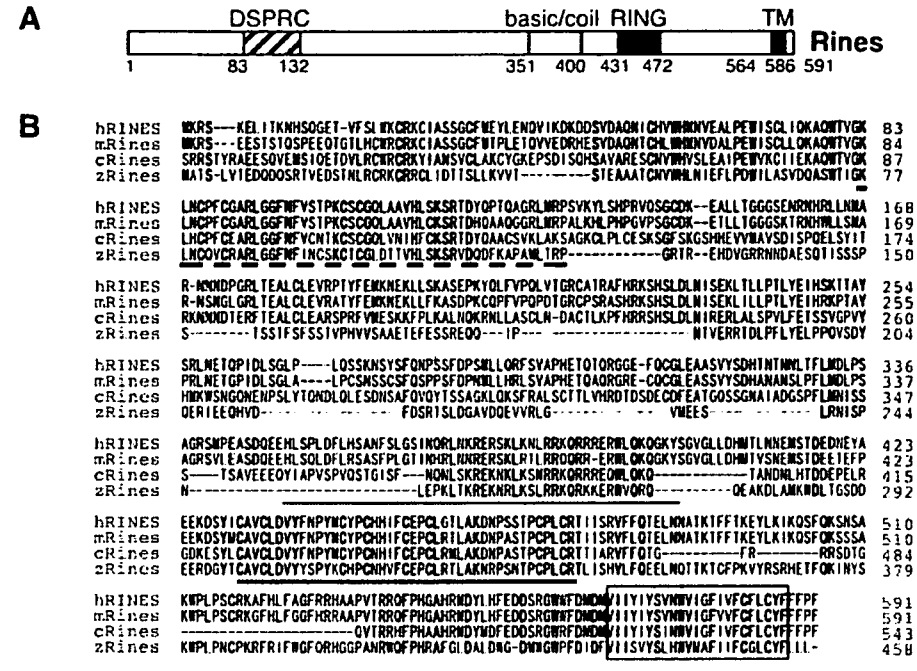

Figure 1 Structure of the Rines. (A) The domain structure of mouse Rines *DSPRC*, dual specificity protein phosphatase Rines conserved domain; basic/coil, basic coiled-coil domain; RING, RING finger domain; TM, transmembrane domain. (B) Alignment of the amino acid sequences of the human (accession: CAD89939), mouse (accession: AAH46775), chick (accession: XP_429137), and zebrafish (accession: NP_956723) Rines. Dark green boxes indicate the conserved amino acids across the four species, and light green boxes indicate the conserved amino acids among the three species. Open box, transmembrane domain; thick underline, RING finger domain; thin underline, basic coiled-coil domain; broken underline, DSPRC domain. (C) Comparison of the RING finger domain amino acid sequences between mouse *Rines*, human *TRIM2*, human *SMARCA3* and human *BRCA1*. (D) Comparison of DSPRC domain sequences derived from rat glucokinase-associated phosphatase (*T-DSP4*, NP_071584), an *Apis mellifera* protein (*Apis*, XP_396430), *Saccharomyces cerevisiae* Yvh1p (*Yvh1*, NP_012292), and *Arabidopsis thaliana* dual specificity protein phosphatase-related protein (*Arabi*, NP_5678561).

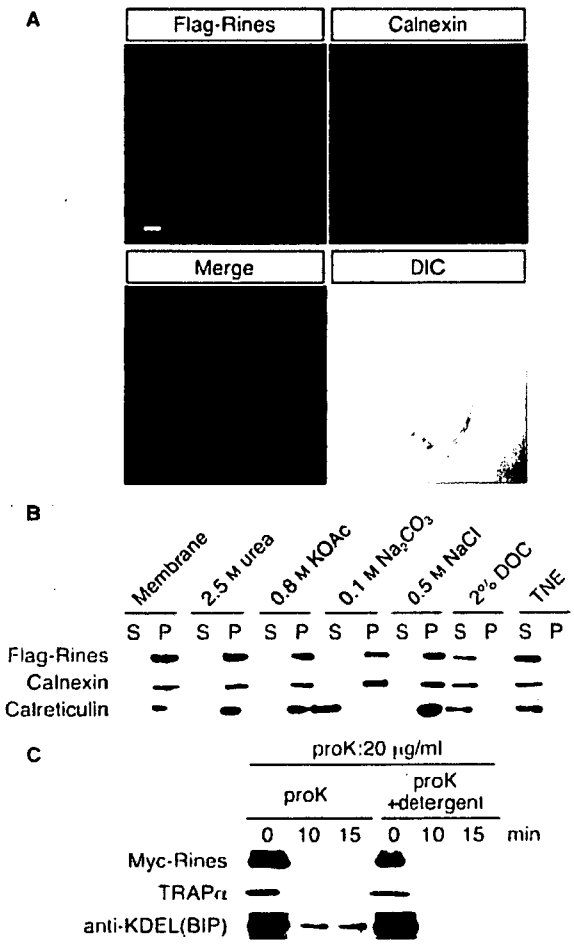

Figure 2 Localization of Rines in cultured cells. (A) Immunofluorescence staining of COS7 cells expressing Flag-Rines. Anti-Calnexin antibody was used to stain a typical ER membrane protein. Blue indicates DAPI-stained nucleus. Scale bar, 5 μm. (B) Membrane preparations of 293T cells expressing Flag-Rines were extracted with buffer containing the materials indicated. *TNE* buffer (150 mM Tris–HCl, pH 7.5; 500 mM NaCl; 1 mM EDTA; 1% Triton X-100; 0.1% SDS), P, pellet; S, supernatant. Each fraction was subjected to immunoblotting with antibodies against Flag-epitope, Calnexin (an integral membrane protein in ER) and Calreticulin (a peripheral membrane protein in ER). (C) N-termini of the Rines are oriented mostly toward the cytoplasm. Protease protection assay of N-terminally Myc-tagged Rines, an ER luminal control *BiP* (Grp78) and an integral ER membrane protein *TRAPα*. The crude membrane fraction prepared from 293T cells expressing Myc-Rines was treated with only proteinase K or with proteinase K with detergent buffer (TNE) for the time indicated. Samples were subjected to immunoblotting using the antibodies indicated.

staining using brains from E13.5 to E17.5 mouse embryos. Throughout these stages, a high level of *Rines* expression was detected in ventricular zone of the lateral ventricle while a low level of expression could be observed throughout other brain region (Fig. 3C–G). At E13.5, the *Rines* expression was detected in a thick layer facing the lateral ventricle, and the expression continued in the ventricular zone at E15.5 through E17.5 (Fig. 3C–G), but the stained layer was thinner at the later stages. In addition, Rines was expressed strongly by lens-forming cells (Fig. 3D). In the sagittal section of E17.5, the *Rines* expression was detected in the olfactory bulb, the ventricular layers facing both on the lateral ventricle and the fourth ventricle and weakly in the thalamus (Fig. 3F). A higher magnification of the cerebral cortex revealed that the *Rines* expression was restricted to the ventricular zone (Fig. 3G).

Rines has a protein-degradation activity dependent on proteasomal function

Because Rines was first found as a Zic2 binding protein in yeast, we performed GST pull-down experiments with the total cell extract from cells transfected with Flag-Rines and GST-fused Zic2 FL (full-length). The precipitates were immunoblotted to detect Flag-Rines (Fig. 4A). We obtained GST-fusion Zic2-bound Rines. To test if the interaction occurs between the purified proteins, we prepared a GST fusion protein containing the Rines fragment obtained from two-hybrid screening (two-hybrid binding region (TBR: 282–489), Fig. 4C) and used this fusion protein for GST pull-down experiments with purified Flag-2HA-Zic2 expressed in, and purified from, 293T cells (Fig. 4B). As a result, we could observe the interaction of GST-Rines-TBR with Flag-2HA-Zic2 (Fig. 4B). This result confirmed that Rines can directly interact with Zic2. Mapping of the Zic2 binding domain in TBR282–489 revealed that both the basic coiled-coil domain and the RING finger domain were involved in the binding (Fig. 4C,D).

To test whether Rines can affect the protein amount of the interacting protein, 293T cells were co-transfected with Flag-Rines and HA-Zic2. We found that the amount of HA-Zic2 in the cell lysate was reduced only when Flag-Rines was co-transfected (Fig. 5A, Input lane2). We then speculated that Rines may be involved in proteasomal protein degradation, because a large number of proteins with the RING finger motif participated in proteasomal protein degradation. This idea led us to examine the HA-Zic2 protein amount in the cells treated with an inhibitor of proteasome function (MG132) or an inhibitor of lysosomal cysteine protease

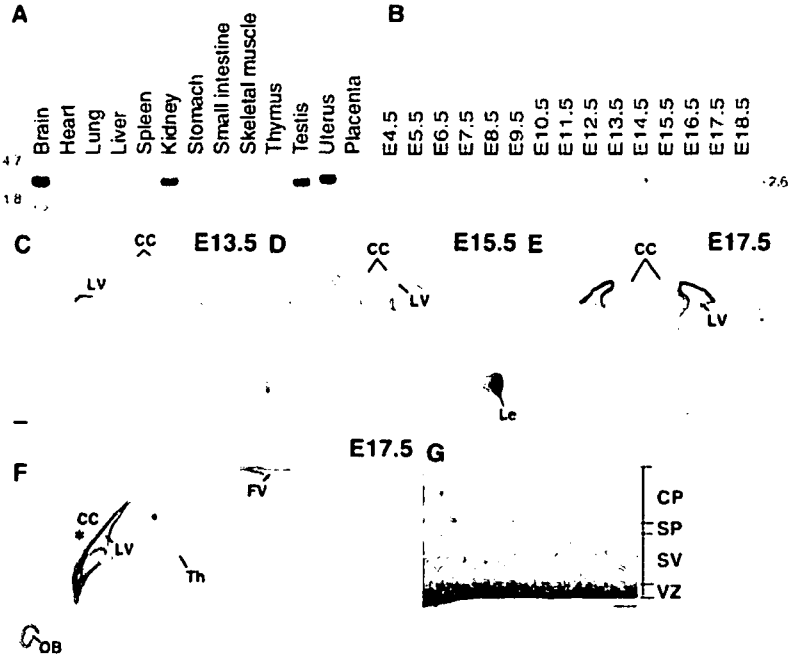

Figure 3 Expression of the Rines. (A–B) Northern blot analyses of a ^{32}P-labeled DNA probe of *Rines*. Each lane contains 20 μg of total RNA. (A) Tissue distribution of the *Rines* mRNA in adult mice. RNA derives from indicated organs of ICR mouse, age 6–10 weeks. (B) Developmental changes in the *Rines* mRNA expression in the mouse embryo from E4.5 to E18.5. (C–G) *in situ* hybridization analysis. *Rines* mRNA distribution is shown in brain sections from E13.5 (C), E15.5 (D), E17.5 (E, F, G) embryos. C–E show coronal sections and F and G show sagittal sections. (G) Higher magnification of the area indicated by asterisk in (F). CC, cerebral cortex; CP, cortical plate; FV, fourth ventricle; Le, lens; LV, lateral ventricle; OB, olfactory bulb; SP, subplate; SV, subventricular zone; Th, thalamus; VZ, ventricular zone. Scale bar, 200 μm.

(E64). As shown in Fig. 5A, the HA-Zic2 in the input lysate decreased in the cells transfected with Flag-Rines was recovered in the cells with MG132 treatment. Similarly, the level of Flag-Rines itself was also increased by the treatment with MG132, but not with E64. In addition, the interaction of Flag-Rines and HA-Zic2 was observed in cells only when the cells were treated with MG132 but not with E64. These results suggest that the apparent absence of the Flag-Rines–HA-Zic2 complex in the cell lysate without MG132 may be due to the rapid degradation of this complex in the proteasome.

To further investigate whether Flag-Rines promotes the degradation of the interacting protein by the proteasome pathway, we examined the Zic2 amount by immunoblot analysis in cells using a series of proteasomal inhibitors or a calpain inhibitor (Fig. 5B). HA-Zic2 was co-transfected into cells with either Flag-Rines or Flag-tagged control vector. The result showed that the Rines-induced degradation of Zic2 was blocked in the presence of the all tested proteasome inhibitors including MG132, Epoxomicin, *clasto*-Lactacystin-β-lactone, Lactacystin and ALLN (Fig. 5B), but was not blocked even in the presence of the high concentration (1 μM) of the calpain inhibitor, Calpastatin peptide (IC50 = 20 nM, Eto *et al.* 1995) (Fig. 5B). These results confirm that Rines promotes the degradation of protein by the proteasome pathway.

To clarify whether or not the Flag-Rines-induced decrement of HA-Zic2 is due to the enhanced Zic2 degradation, we performed a cycloheximide chase experiment. HA-Zic2 was co-expressed in cells with either Flag-Rines or Flag-vector control. Cycloheximide was added 26 h after transfection to inhibit new protein synthesis, and cells were harvested at the indicated time points. The decay of HA-Zic2 was analyzed by immunoblotting. A clear effect on the stability of HA-Zic2 was observed in this cycloheximide chase experiment (Fig. 5C,D). In the presence of the Flag-Rines, the level of HA-Zic2 severely decreased at 4 and 6 h after cycloheximide addition, whereas this effect was not seen in the absence of Flag-Rines. These results indicate that Flag-Rines indeed shortens the half-life of HA-Zic2. We also observed a rapid decrement of Rines itself (Fig. 5C) in accord with the proteasomal degradation of Flag-Rines (Fig. 5A).

Rines can bind to a ubiquitin-conjugating E2 enzyme and shows ubiquitin-ligase activity

The RING finger motifs in RING-type E3s have been shown to serve as recruiting motifs for specific E2 ubiquitin-conjugating enzymes. It was considered that Rines is involved in the proteasomal machinery. To test whether Rines could recruit an E2-ubiquitin conjugating

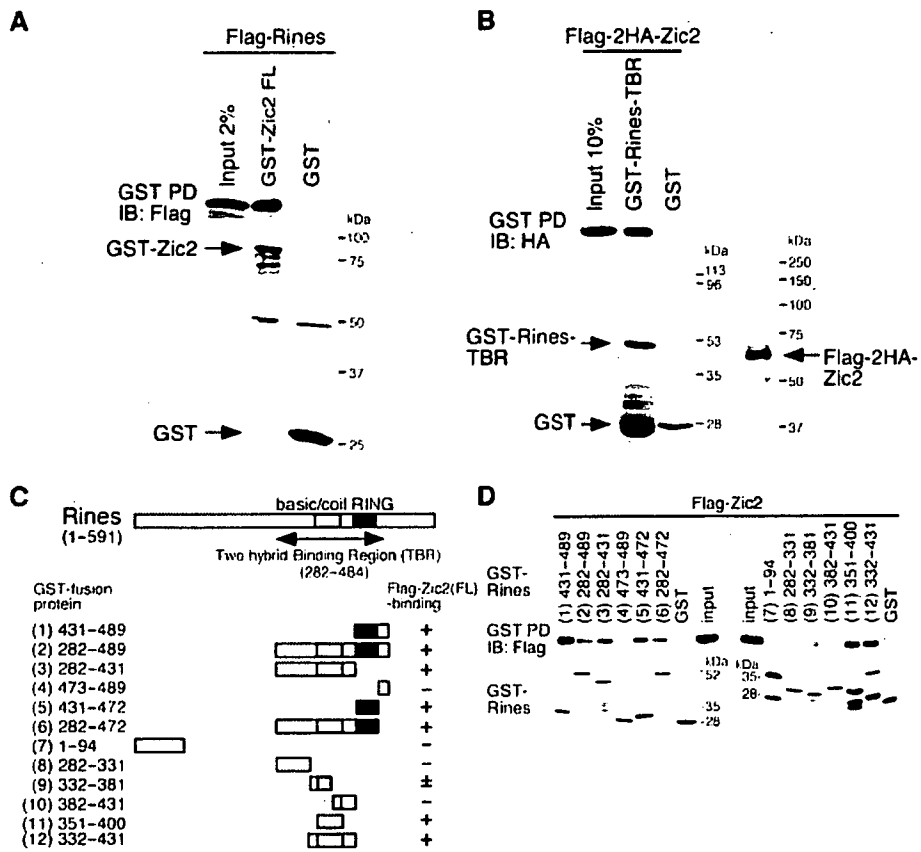

Figure 4 Zic2-binding activity of Rines. (A) Rines binds Zic2 *in vitro*. 293T cells were transfected with Flag-Rines, and the cell lysates containing equal amount of proteins were incubated with the GST-Zic2. The eluates from the glutathione sepharose beads were analyzed by immunoblotting with anti-Flag antibody (upper panel). GST-Zic2 was shown as amido black staining (lower panel). (B) Rines directly interact with Zic2. Flag-2HA-Zic2 expressed and purified from 293T cells was incubated with the GST-Rines-TBR (282–489) fusion protein or GST protein and GST pull-down assay was performed. Bound material was detected by immunoblotting using anti-HA antibody. GST-Rines-TBR fusion protein was shown as amido black staining (lower left panel). The input purified Flag-2HA-Zic2 was shown as silver staining (lower right panel). (C–D) Rines binds Zic2 in the basic coiled-coil domain and RING finger domain. (C) A schematic representation of the Rines, its deletion mutants and the result of mapping of the Zic2-binding region in Rines. The various regions of the Rines were prepared as GST fusion proteins. The numbers refer to amino acids. (D) GST pull-down assays. Upper panel, immunoblot using anti-Flag antibody; lower panel, amido black staining indicating GST-Rines deletion proteins.

enzyme, we performed a GST pull-down assay using GST-Rines-TBR, which contains the RING finger motif, and a set of the Myc-E2s (UbcH5a, H5b, H5 c, H6, H7 and H8) expressed in cells (Fig. 6A). As a result, GST-Rines-TBR associated with Myc-UbcH6, but not with Myc-UbcH5a, H5b, H5c, H7 or H8.

It is known that almost all known RING-type E3 ligases themselves are susceptible to be ubiquitinated (Fang & Weissman 2004). Overexpression of Myc- or Flag-Rines in 293T, NIH 3T3 and COS7 cells resulted in the formation of higher molecular weight bands that were recognized by immunoblot using anti-Myc or Flag antibodies (data not shown). We then examined whether Rines could be covalently modified by ubiquitin (Fig. 6B). An expression plasmid encoding a HA-ubiquitin was transfected into NIH 3T3 cells with or without plasmid for Flag-Rines, followed by immunoprecipitation with anti-Flag antibody. An immunoblot analysis of immunoprecipitates with anti-HA antibody showed a broad band with high molecular weight only when HA-ubiquitin and Flag-Rines were co-expressed. When the same samples were immunoblotted with anti-Flag antibody, the broad bands with high molecular weight appeared regardless of the presence of HA-ubiquitin. These results

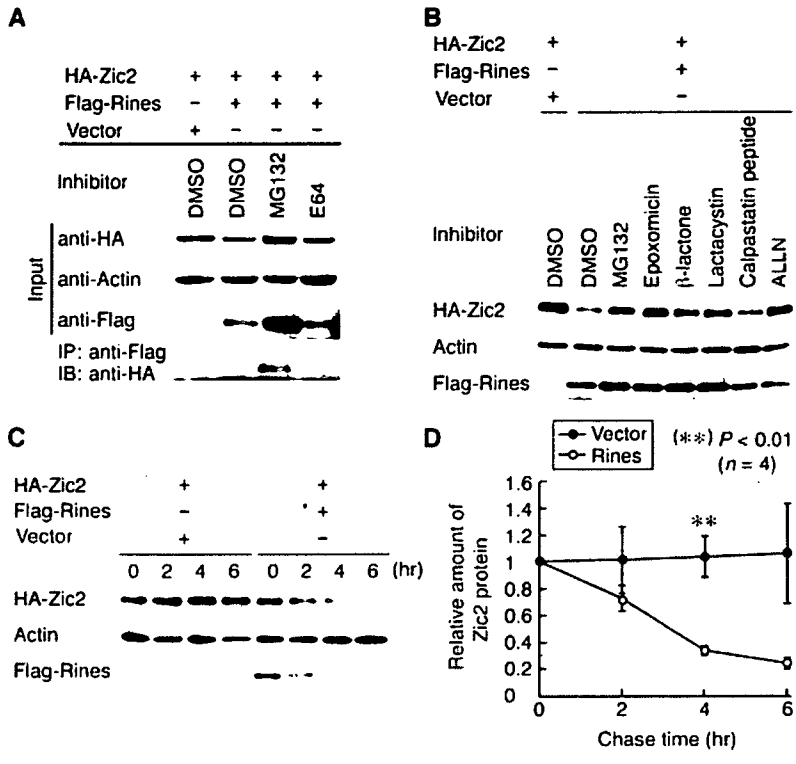

Figure 5 Proteasomal degradation-enhancing activity of Rines. (A) Co-immunoprecipitation of Rines with Zic2 from transfected cells. 293T cells were co-transfected with indicated vectors, and cultured with dimethylsulfoxide (DMSO), proteasome inhibitor MG132 (20 μM), or lysosomal protease inhibitor E64 (50 μM). An equal amount of protein from each cell lysate was subjected to immunoprecipitation and immunoblotting using the antibodies indicated (bottom panel). Expression analysis of the HA-, Flag-tagged gene products and actin protein (as internal control) was done by immunoblotting of the cell extracts (top three panels). The protein ratio used for immunoprecipitation and immunoblotting lanes was 40 : 1. (B) The effects of Rines on Zic2 degradation were blocked by the proteasome inhibitors but not the calpain inhibitor. NIH 3T3 cells were co-transfected with indicated vectors, and were treated with the proteasome inhibitor, MG132 (10 μM), Epoxomicin (10 μM), *clasto*-Lactacystin-β-lactone (10 μM), Lactacystin (20 μM), ALLN (25 μM), the calpain inhibitor, Calpastatine peptide (1 μM) or vehicle (DMSO). The cell lysates were analyzed by immunoblotting. (C–D) Rines accelerates Zic2 turnover. (C) NIH 3T3 cells were transfected with indicated vectors and cultured with cycloheximide. The cell lysates prepared at 0, 2, 4 and 6 h after cycloheximide treatment were analyzed by immunoblotting with anti-HA, anti-Flag or anti-actin antibodies. (D) Relative amount of Zic2. The Zic2 amounts have been normalized to actin so that the value for the amounts at 0 h equals 1.0. The plots indicate means of four independent analyses. Error bars represent standard error. Asterisk denotes statistical significance in the Zic2 amount between the Flag-Rines-transfected and the control vector-transfected cell lysates. **, $P < 0.01$, $n = 4$, by Student's *t*-test.

indicate that Flag-Rines is heavily ubiquitinated and Flag-Rines can be modified with endogenous ubiquitin as well as exogenous ubiquitin.

Next, we tested whether Rines has an ubiquitin ligase activity (Fig. 7A). Flag-Zic2 was co-transfected into NIH 3T3 cells along with HA-tagged ubiquitin in the absence or presence of a plasmid with Myc-tagged Rines. Cell lysates were subjected to immunoprecipitation with an anti-Flag antibody, followed by immunoblotting with an anti-HA antibody to detect ubiquitin-conjugated Zic2. A broad band with high molecular weight was more enhanced in the presence of Myc-Rines than in its absence. Accordingly, the ubiquitination of endogenous Zic2 was enhanced by Myc-Rines in rat neural stem cell line MNS70 cells (Fig. 7B). These results indicate that Rines can promote the polyubiquitination of the interacting protein. Furthermore, deletion of the RING finger motif abolished the ability of Rines to promote the ubiquitination of endogenous Zic2 – the ability integral Rines possesses (Fig. 7B). Because the RING finger motif is suggested to be essential for the enzymatic activity of RING-type E3 ubiquitin ligase (Joazeiro & Weissman

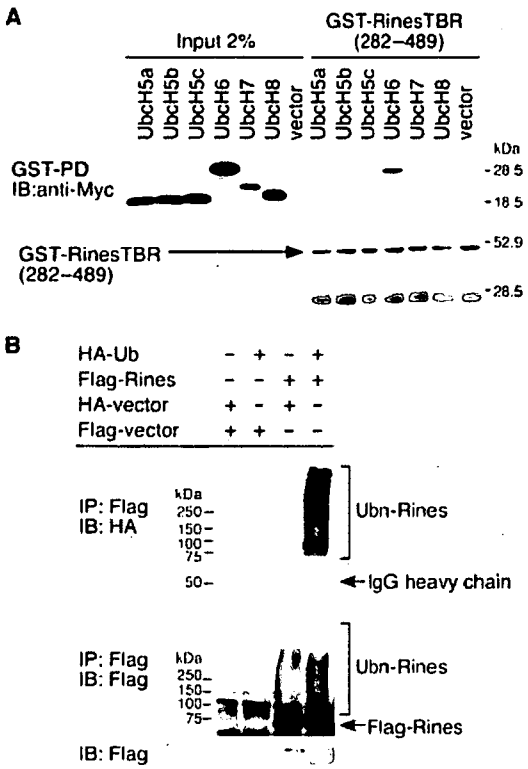

Figure 6 Rines can bind to a ubiquitin-conjugating E2 enzyme and can be polyubiquitinated. (A) Rines binds selectively to UbcH6. Extracts from 293T cells expressing the ubiquitin-conjugating E2 enzymes (Myc-UbcH5a, H5b, H5c, H6, H7, H8) were subjected to GST pull-down assay using the GST-Rines-TBR fusion product, and detected with anti-Myc antibody (upper panel). GST-Rines-TBR fusion product was shown as amido black staining (lower panel). (B) Rines is polyubiquitinated in NIH 3T3 cells. NIH 3T3 cells were transfected with the plasmids indicated. An equal amount of protein from each cell lysate was immunoprecipitated with anti-Flag antibody and then immunoblotted with anti-HA or anti-Flag antibodies to detect ubiquitinated proteins as smear bands (upper two panels). Expression analysis of Flag-Rines by immunoblotting of cell extracts (bottom panel). The protein ratio used for the immunoprecipitation and immunoblotting lanes was 65 : 1.

2000; Pickart 2001), these results support the hypothesis that Rines is an E3 ubiquitin ligase. In addition, we observed the interaction of endogenous Zic2 with both Myc-Rines and Myc-ΔRING (Fig. 7B) in the immunoprecipitation assay. This result is consistent with the *in vitro* binding to Zic2 by Rines (Fig. 4C,D) and the co-immunoprecipitation of Rines with Zic2 (Fig. 5A). These results suggest that Rines can promote the ubiquitination of the interacting protein.

Discussion

Rines gene-encoded product is a novel member of the RING finger protein family and functions as an E3 ubiquitin ligase

Rines contained two functional domains, a C3HC4-type RING finger domain and a basic coiled-coil domain, both of which can act as protein binding domain. As with many other RING-type E3 ligases, the RING finger motif of Rines may function as a recruiting motif for an E2 ubiquitin-conjugating enzyme, UbcH6, because Rines-TBR, which contains the RING finger motif, can bind UbcH6. In addition, the RING finger motif of Rines is required for its protein ubiquitination activity. These results support the inference that Rines functions as an E3 ubiquitin ligase. The coiled-coil domain is known to participate in homo-multimerization of proteins and protein–protein interaction (Jensen *et al.* 2001; Reymond *et al.* 2001). Interestingly, co-existence of the RING domain and the coiled-coil domain is also found in RBCC/TRIM proteins, the RING finger domain of which is similar to that of Rines (Fig. 1C), and in which coiled-coil domains play a role in homo-multimerization and the cell compartment-specific distribution of proteins (Reymond *et al.* 2001; Dho & Kwon 2003). In addition, co-existence of the RING domain and the coiled-coil domain was reported in Staring, which is an E3 ubiquitin ligase targeting syntaxin (Chin *et al.* 2002). In this case, the coiled-coil domain acts as the substrate-binding domain. The finding that the coiled-coil domain can bind a protein is consistent with the macromolecular assembling properties of this domain.

As to the molecular function of Rines, we revealed that Rines functions as an E3 ubiquitin ligase on the basis of the following three facts: (i) Flag-Rines promote the proteasomal degradation of the interacting protein, (ii) Myc-Rines enhance the ubiquitination of the interacting protein, and (iii) GST-Rines-TBR associates with an E2 ubiquitin-conjugating enzyme (Myc-UbcH6). Furthermore, Flag-Rines itself is heavily ubiquitinated and degraded by proteasome as are the case in many other E3 ubiquitin ligase (Fang & Weissman 2004). A rapid degradation of Flag-Rines itself was also observed in cycloheximide chase experiments. This may explain why we could not detect endogenous Rines protein in brain lysates by using anti-Rines antibodies, which could detect over-expressed Rines in cultured cells treated with a proteasome inhibitor (data not shown).

In terms of other molecular properties of Rines, its location in the ER membrane is intriguing. Recent studies of the ER-associated protein degradation (ERAD)

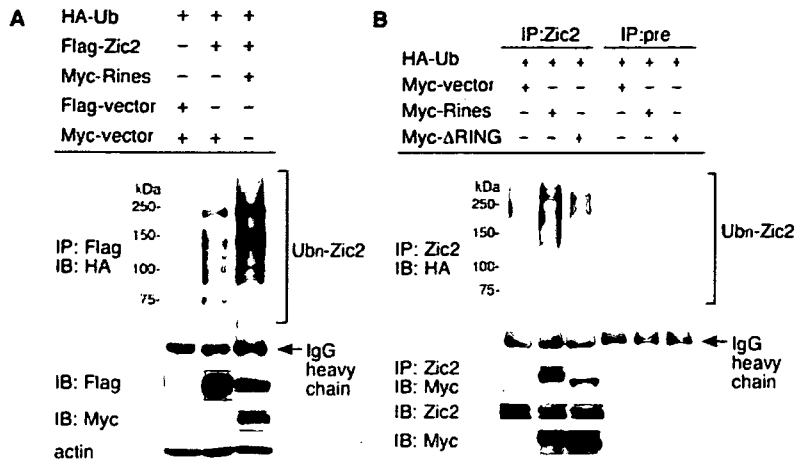

Figure 7 Rines shows ubiquitin-ligase activity. (A) NIH 3T3 cells were transfected with the plasmids indicated. An equal amount of protein from each cell lysate was immunoprecipitated with anti-Flag antibody and then immunoblotted with anti-HA antibody to detect ubiquitinated proteins as smear bands (upper panel). Expression analysis of Flag- and Myc-tagged gene products and actin protein, respectively, by immunoblotting of cell extracts (bottom three panels). The protein ratio used for the immunoprecipitation and immunoblotting lanes was 30 : 1. (B) Rines promotes the ubiquitination of endogenous protein in a RING finger domain-dependent manner. MNS70 cells were transfected with the plasmids indicated and cultured with a proteasome inhibitor (epoxomicin). An equal amount of protein from each cell lysate was immunoprecipitated with anti-Zic2 antibody and then immunoblotted with anti-HA antibody to detect ubiquitinated Zic2 (top panel) and with anti-Myc antibody to detect the interaction of Zic2 and Rines (second from the top panel). Zic2 protein and Myc-tagged Rines in the cell extracts were confirmed by immunoblotting (bottom two panels). The protein ratio used for the immunoprecipitation and immunoblotting lanes was 10 : 1.

system have shown that this system is an essential protein proofreading and elimination system (Kostova & Wolf 2003). Studies in yeast have shown that the RING-finger-domain-containing ER integral membrane proteins Der3/Hrd1p and Doa10 cooperate with an E2 ubiquitin-conjugating enzyme, and they are considered to act as E3 ubiquitin ligases in the ERAD pathway (Bays *et al.* 2001; Deak & Wolf 2001; Swanson *et al.* 2001; Deng & Hochstrasser 2006; Ravid *et al.* 2006). Moreover, RING-finger-domain-containing ER membrane proteins, gp78 and RMA1, are considered to be the mammalian orthologs of the yeast ERAD machinery (Fang *et al.* 2001; Younger *et al.* 2006). The RBCC/TRIM protein RFP2 was recently reported to be an ER membrane-anchored ubiquitin ligase involved in the ERAD pathway (Lerner *et al.* 2007). However, it is possible that additional functional homologues exist in vertebrates, considering the increased diversity of functional proteins in vertebrates compared with in yeast. Rines may be a good candidate for a component of the ERAD system in the vertebrate CNS. It is known that Doa10, which resides in the ER/nuclear envelope, degrades the nuclear transcription factor Matα2 as well as ER proteins (Swanson *et al.* 2001; Deng & Hochstrasser 2006; Ravid *et al.* 2006). It is possible that Rines can act in a similar fashion to Doa10 and degrade the substrates of the ERAD pathway as well as nuclear proteins. This possibility should be addressed in a future study.

Possible biological roles of Rines

By using Zic2 as a tool protein that can bind Rines, we demonstrated the proteasomal degradation activity of Rines. However, the biological significance of Rines-mediated Zic2-degradation *in vivo* is unclear, because we did not see a clear increase in Zic2 protein amount in conventional immunoblot or immunofluorescence staining analyses of the brains of *Rines* knockout mice (M. Ogawa and J. Aruga, unpublished observation). Although we cannot exclude the possibility that Rines-mediated Zic2 degradation occurs occasionally, it seems better to postulate that there are other major degradation targets of Rines *in vivo*.

Because the expression of *Rines* is strong in immature neural cells and lens cells, we are interested in the possible degradation targets of Rines in these tissues. In addition, the role of Rines in the mature brain, another major organ showing *Rines* expression, should be clarified.

taking into account emerging roles of the ubiquitin–proteasome pathway in the modulation of neuronal function, such as regulation of synaptic structure and synaptic plasticity (Johnston & Madura 2004; Moriyoshi *et al.* 2004; Yao *et al.* 2007) and in neurodegeneration, such as in Parkinson's disease (Gandhi & Wood 2005) and Alzheimer's disease (Hegde & Upadhya 2007). Although the authentic Rines targets are unclear at this point, the biological significance of Rines is shown by neurobehavioral abnormalities observed in *Rines* knockout mice (M.O., J.A. unpublished observation). Further clarification of the molecular function of Rines is needed for an in-depth understanding of its roles in the proteasomal degradation system in mammalian brains.

Experimental procedures

Yeast two-hybrid screening

Yeast two-hybrid screening was done according to (Mizugishi *et al.* 2004) using an amino-terminal region of mouse Zic2 (amino acid number 1–255) as a bait protein.

cDNA cloning and plasmid construction

Full-length mouse *Rines* cDNA (accession: AAH46775) was cloned by using cDNA library screening and PCR. The cDNA fragment from a cDNA clone obtained in the two-hybrid screening was used for the screening of mouse cerebellum λ-gt11 cDNA library (gifted by Dr T. Furuichi). We obtained the partial cDNA fragment of the *Rines* gene by the screening. Then, 5′ end of the mouse *Rines* cDNA was cloned from E15 mouse embryonic brain cDNAs by using the PCR. The primers used were 5′-TAG CAGCTAATCTCGGTTGC-3′, derived from NCBI database accession: AK013941 and, 5′-GGACATGCACTGATCAGTAA-3′, derived from the cDNA fragment obtained by library screening. The PCR conditions were 35 cycles of 94 °C for 15 min, 58 °C for 1 min and 72 °C for 2 min. The expression vector Flag-Rines was constructed by inserting the entire protein-coding region of *Rines* in-frame into the AviII/SrfI-EcoRI site of pCMVtag2 (Stratagene, La Jolla, CA).

To express Flag-tagged, hemagglutinin (HA)-tagged, and Myc-tagged proteins, the relevant sequences were amplified by PCR, verified by DNA sequencing, and subcloned into pCMVtag2 (Stratagene), pcDNA3HA (a gift from Dr T. Nakajima), and pCS2 + MT (Turner & Weintraub 1994). For the Myc-Rines construct, full-length *Rines* (1–591) was amplified by PCR and digested with *Eco*RI into pCS2 + MT. In the case of Rines-ΔRING-(431–472), two fragments (1–430 and 473–591) amplified by PCR were digested with *Xho*I-*Bgl*I and *Bgl*I-*Xho*I, joined together, and then inserted into pCS2 + MT The GST-Zic2 was constructed by inserting the cDNA fragment containing the entire ORF of mouse Zic2 into the EcoRI site of pGEX-4T3 vector (GE Healthcare, Uppsala, Sweden). For the GST-Rines-deletions constructs, fragments were amplified by PCR using primers that contain BamHI-EcoRI sites, sequenced, and cloned into the BamHI- EcoRI sites of the pGEX-4T1 vector (GE Healthcare).

HA-Zic2 and Flag-Zic2 were constructed by inserting the cDNA fragment containing the entire ORF of mouse Zic2 into the BamHI-EcoRI site of pcDNA3HA or pCMVtag2 (Mizugishi *et al.* 2001). The Flag-2HA-Zic2 was constructed by inserting the cDNA fragment containing the two tandem repeat of hemagglutinin (HA) into the SrfI-BamHI site of pCMVtag2-Flag-Zic2. The construction of Myc-tagged UbcH5a, H5b, H5c, H6, H7, H8 and HA-tagged Ubiquitin expression vectors will be described elsewhere.

Cell culture and transfection

293T, COS7 and NIH 3T3 cells were maintained at 37 °C with 5% CO_2 in Dulbecco's Modified Eagle's Medium (DMEM, Sigma, St Louis, MO) supplemented with 10% fetal bovine serum (FBS). MNS70 cells (rat neural stem-derived cells, Nakagawa *et al.* 1996) were maintained at 37 °C with 5% CO_2 in a 1 : 1 mixture of DMEM and F12 medium (DF; Sigma) supplemented with 10% FBS, 5% horse serum (HS), and antibiotics. The cells were plated at a density of 3.5×10^4 cells/cm^2 24 h before transfection. 293T and COS7 cells were transfected with Effectene transfection reagent (Qiagen, Valencia, CA) or Trans-IT-LT1 transfection reagent (Mirus, Madison, WI), NIH 3T3 cells were transfected with Superfect transfection reagent (Qiagen) or Lipofectamine Plus or 2000 transfection reagent (Invitrogen, Carlsbad, CA), and MNS70 cells were transfected with Fugene HD transfection reagent (Roche, Basel, Switzerland), according to the manufacturer's instructions.

Immunoblotting

The proteins and gene products were separated by 7.5%–15% SDS-polyacrylamide gel electrophoresis (SDS-PAGE) and transferred to PVDF membrane (Immobilon, Millipore, Bedford, MA). The membranes were immersed in 3%–6% skim milk overnight at 4 °C and incubated with first antibody. The bound antibodies were detected using horseradish peroxidase-conjugated secondary antibodies (anti-mouse, rabbit or rat IgG) and ECL reagents (GE Healthcare).

Subcellular localization studies

COS7 cells were transiently transfected with Flag-Rines. Cells were fixed at 24 h after transfection in 4% paraformaldehyde in 0.1 M sodium phosphate buffer for 15 min at room temperature, incubated with blocking buffer (5% bovine serum albumin in phosphate-buffered saline) for 1 h at room temperature and then incubated overnight at 4 °C with the anti-Calnexin antibody (Stressgen, San Diego, CA) and anti-Flag M2 monoclonal antibody (Sigma) diluted with buffer (0.3% triton X-100 and 1% bovine serum albumin in phosphate-buffered saline). The bound antibodies were detected by Alexa 488-conjugated anti-mouse IgG or Alexa 594-conjugated anti-rabbit IgG antibodies (Molecular Probes Inc., Eugene, OR).

Membrane preparation and protease protection assay

The membrane fraction was prepared as described (Lenk *et al.* 2002). For microsomes of Flag–Rines-transfected 293T cells, cells were scraped 24 h after transfection and then washed once in PBS and homogenized in a homogenization buffer (50 mM Tris–HCl, pH 7.5, 250 mM sucrose, 2 mM EDTA, 150 mM KCl, 1 mM DTT and complete protease inhibitor cocktail (Roche)). The cell lysates were centrifuged at 3000 *g* for 10 min at 4 °C. After centrifugation at 10 000 *g* for 15 min, the supernatant was subsequently centrifuged at 75 000 *g* for 60 min and the pellet (microsome fraction) was resuspended in a membrane buffer (150 mM sucrose, 50 mM Hepes, pH 7.5, 2.5 mM MgOAc, 50 mM KOAc and protease inhibitors) or a membrane buffer containing 2.5 M Urea, 800 mM KOAc, 0.1 M Na_2CO_3, 500 mM NaCl or 2% sodium deoxycholate or TNE buffer (150 mM Tris–HCl, pH 7.5, 500 mM NaCl, 1 mM EDTA, 1% Triton X-100, 0.1% SDS). The cell suspensions were centrifuged at 18 000 *g* for 60 min, then the pellets were resuspended in preboiled SDS-lysis buffer (50 mM Tris–HCl, pH 7.5, 0.5 mM EDTA, 1% SDS, 1 mM dithiothreitol), boiled for an additional 10 min and diluted 10-fold by adding 0.5% NP-40 buffer. A protease protection assay was performed according to the method of Sommer and Jentsch (1993). Myc-Rines-transfected 293T cells were homogenized in the homogenization buffer without EDTA or protease inhibitor and then centrifuged at 3000 *g* for 10 min at 4 °C. The crude homogenates were treated with protease K (20 μg/mL), or untreated, in the presence or absence of detergent buffer (TNE). The following antibodies were used in this study: anti-Flag (M2, Sigma), anti-Myc (9E10, Santa Cruz Biotechnology), anti-Calnexin (BD Biosciences, La Jolla, CA), anti-Calreticulin (BD Biosciences), anti-TRAPα (Upstate, Lake Placid, NY), anti-KDEL (Stressgen).

Northern blot analysis

Two types of Northern blot sheets (Mouse Adult Tissue Blot, Mouse Embryo Full Stage Blot, Seegene, Seoul, Korea) were used to determine the expression profiles of the mouse *Rines* genes. ^{32}P-labeled Rines cDNA probe corresponding to the 1.1 kb fragment of Rines cDNA, from the last RING finger motif toward the 3′untranslated region was synthesized with Random Primed DNA Labeling Kit (Roche). The hybridizations were performed in a buffer consisting of 0.5 M Na_2HPO_4, pH7.2, 7.0% SDS, 1% BSA, 1 mM EDTA, pH8.0, 100 μg/mL herring sperm DNA at 65 °C overnight. These membranes were washed 3 times with 2 × SSC–0.1% SDS at room temperature for 5 min, and finally washed with 0.1 × SSC–0.1% SDS at 56 °C for 40 min, and X-ray films were exposed to the washed membrane with an intensifying screen for 24 h to 7 days. The images were digitized, and the contrast and brightness were optimized.

In situ hybridization

The expression of the *Rines* in the developing animal was investigated in ICR mice purchased from Nihon SLC (Shizuoka, Japan). All animal experiments were carried out according to the guidelines for animal experimentation in RIKEN. *In situ* hybridizations were performed was done as previously described (Nagai *et al.* 1997). Same probe for *Rines* in the Northern blot analysis was used. The specificity of the hybridization signals was verified by the absence of any signals in a control hybridization performed with a *Zic2* sense-strand probe (Nagai *et al.* 1997).

GST pull-down assay

Flag-2HA-Zic2 was purified from 293T cells that were transiently transfected with pCMV-Flag-2HA-Zic2 (Ishiguro *et al.* 2007). Produced protein was affinity-purified with anti-HA agarose beads (Sigma) and HA-peptide (100 ng/mL, Sigma), followed by subsequent affinity purification using anti-Flag agarose beads (Sigma) and Flag-peptide (100 ng/mL, Sigma).

293T cells were transiently transfected with Flag-Rines, Flag-Zic2 or Myc-ubiquitin-conjugating E2 enzyme expression vectors. Cells were harvested 24 h after transfection and were lysed in an immunoprecipitation buffer A (25 mM Hepes, pH 7.2, 0.5% NP-40, 150 mM NaCl, 50 mM NaF, 2 mM Na_3VO_4, 1 mM phenylmethylsulfonyl fluoride, and 20 μg/mL aprotinin) or buffer B (20 mM Hepes, pH 7.4, 150 mM NaCl, 5 mM EDTA, 10% glycerol, 0.5% Triton X-100, 0.5 mM N-ethylmaleimide, 0.5 mM iodoacetamide, 1 mM phenylmethylsulfonyl fluoride and 20 μg/mL aprotinin and contained with 0.1 mg/mL BSA in the case of the direct binding assay). After a centrifugation at 15 000 *g* for 15 min, these supernatant and Flag-2HA-Zic2 were incubated for 2 h at 4 °C with appropriate GST-fusion proteins, and then added with 20 μL of 50% suspension of Glutathione Sepharose 4B beads and incubated for another 2 h at 4 °C. After washing 5 times with the same immunoprecipitation buffer, bound proteins were separated by SDS-PAGE, immunoblotted with the anti-Flag M2 monoclonal antibody (Sigma) or anti-HA Y-11 polyclonal antibody (Santa Cruz Biotechnology, Santa Cruz, CA), or anti-HA 3F10 rat monoclonal antibody (Roche), and detected by ECL system (GE Healthcare).

Immunoprecipitation assay

293T cells were transfected with HA-Zic2 and Flag-Rines or Flag-tagged vector. 48 h after transfection, the cells were treated with the proteasome inhibitor MG132 (Carbobenzoxy-Leu-Leu-Leu-CHO, 20 μM; Calbiochem, San Diego, CA), E64 (50 μM; Sigma) or vehicle Me_2SO; DMSO (final concentration (0.2%)) for 12 h. Cells were then lysed in the immunoprecipitation buffer A (described above) and the lysate was centrifuged at 15 000 *g* for 15 min. These supernatant were incubated for 2 h at 4 °C with a 25 μg of anti-Flag M2 monoclonal antibody (Sigma), and then incubated for another 2 h at 4 °C after adding 20 μL of 50% suspension of protein G agarose beads (Pierce). After washing 5 times with the buffer A, the bound proteins were analyzed by SDS-PAGE and immunoblotting as described above.

Degradation assay

NIH 3T3 cells were transfected with HA-Zic2 and Flag-Rines or Flag-tagged control vector. Cells were treated 43 h after transfection

with the proteasome inhibitor, MG132 (10 μM), Epoxomicin (10 μM; Boston Biochem, Cambridge, MA), clasto-Lactacystin-β-lactone (10 μM; BostonBiochem), Lactacystin (20 μM; BostonBiochem or PeptideInstitute, Osaka, Japan), ALLN (Ac-Leu-Leu-Nle-CHO (MG101), 25 μM; Calbiochem), the calpain inhibitor, Calpastatine peptide (1 μM; Calbiochem) or vehicle (DMSO, at a final concentration of 0.2%) for 9 h. The cell lysates were subjected for immunoblotting.

Cycloheximide chase assay

NIH 3T3 cells were transiently co-transfected with HA-Zic2 and Flag-Rines or Flag-tagged vector as described in a degradation assay. 26 h after transfection, culture medium was replaced by DMEM with 10% FBS containing cycloheximide (25 μg/mL). Cells were washed and harvested with PBS(−) buffer 0, 2, 4, 6 h after addition of cycloheximide, lysed and followed by immunoblotting. HA-Zic2 bands and actin bands were densitometrically quantified with NIH Image (v1.61, <http://rsb.info.nih.gov/nih-image/>), and HA-Zic2 amounts were normalized to actin amounts at each time point.

In vivo ubiquitination assay

NIH 3T3 cells were transfected with combinations of the following plasmids: HA-ubiquitin, Flag-Rines, Flag-Zic2, Myc-Rines and Flag-, HA-, Myc-tagged control vectors. After 50 h of incubation, the cells were lysed in a lysis buffer (20 mM Hepes, pH 7.4, 150 mM NaCl, 5 mM EDTA, 10% glycerol, 0.5% Triton X-100, 0.5 mM *N*-ethylmaleimide, 0.5 mM iodoacetamide, and 5 nM ubiquitin aldehyde (Calbiochem)) and a complete protease inhibitor cocktail (Roche). The lysates were subjected to immunoprecipitation by using anti-Flag agarose beads (18 μL, Sigma) and to an immunoblot analysis with anti-HA antibody (Roche) or anti-Flag antibody. For the endogenous Zic2 ubiquitination assay, MNS70 cells were transfected with combinations of the following plasmids: HA-ubiquitin, Myc-Rines, Myc-ΔRING, and Myc-tagged control vector. Forty-three hours after transfection, the cells were incubated for 6 h with 5 μM epoxomicin. The cells lysed in the lysis buffer described above, and the lysates were subjected to immunoprecipitation with anti-Zic2 antibody and immunoblot analysis with anti-HA antibody (Roche).

Acknowledgements

We thank Haruhiko Bito for critical comments on manuscript, Takashi Inoue, Kei-ichi Katayama, Naoko Morimura and Takahiko J Fujimi for technical advice and helpful discussions, members of Aruga and Mikoshiba laboratories for helpful discussions and Shigetsugu Hatakeyama for the gift of HA-ubiquitin vector. This work is supported in parts by The Mochida Memorial Foundation of Medical Pharmaceutical Research, and Grants-in-Aid for Scientific Research from Ministry of Education, Culture, Sports, Science and Technology of Japan.

References

Aruga, J., Nagai, T., Tokuyama, T., Hayashizaki, Y., Okazaki, Y., Chapman, V.M. & Mikoshiba, K. (1996) The mouse *zic* gene family. Homologues of the *Drosophila* pair-rule gene odd-paired. *J. Biol. Chem.* **271**, 1043–1047.

Bays, N.W., Gardner, R.G., Seelig, L.P., Joazeiro, C.A. & Hampton, R.Y. (2001) Hrd1p/Der3p is a membrane-anchored ubiquitin ligase required for ER-associated degradation. *Nat. Cell Biol.* **3**, 24–29.

Borden, K.L. (2000) RING domains: master builders of molecular scaffolds? *J. Mol. Biol.* **295**, 1103–1112.

Chin, L.S., Vavalle, J.P. & Li, L. (2002) Staring, a novel E3 ubiquitin–protein ligase that targets syntaxin 1 for degradation. *J. Biol. Chem.* **277**, 35071–35079.

Deak, P.M. & Wolf, D.H. (2001) Membrane topology and function of Der3/Hrd1p as a ubiquitin–protein ligase (E3) involved in endoplasmic reticulum degradation. *J. Biol. Chem.* **276**, 10663–10669.

Deng, M. & Hochstrasser, M. (2006) Spatially regulated ubiquitin ligation by an ER/nuclear membrane ligase. *Nature* **443**, 827–831.

Dho, S.H. & Kwon, K.S. (2003) The Ret finger protein induces apoptosis via its RING finger-B box-coiled-coil motif. *J. Biol. Chem.* **278**, 31902–31908.

Eto, A., Akita, Y., Saido, T.C., Suzuki, K. & Kawashima, S. (1995) The role of the calpain–calpastatin system in thyrotropin-releasing hormone-induced selective down-regulation of a protein kinase C isozyme, nPKCε, in rat pituitary GH4C1 cells. *J. Biol. Chem.* **270**, 25115–25120.

Fang, S., Ferrone, M., Yang, C., Jensen, J.P., Tiwari, S. & Weissman, A.M. (2001) The tumor autocrine motility factor receptor, gp78, is a ubiquitin protein ligase implicated in degradation from the endoplasmic reticulum. *Proc. Natl. Acad. Sci. USA* **98**, 14422–14427.

Fang, S. & Weissman, A.M. (2004) A field guide to ubiquitylation. *Cell Mol. Life Sci.* **61**, 1546–1561.

Fujiki, Y., Hubbard, A.L., Fowler, S. & Lazarow, P.B. (1982) Isolation of intracellular membranes by means of sodium carbonate treatment: application to endoplasmic reticulum. *J. Cell Biol.* **93**, 97–102.

Gandhi, S. & Wood, N.W. (2005) Molecular pathogenesis of Parkinson's disease. *Hum. Mol. Genet* **14**, 2749–2755.

Giaever, G., Chu, A.M., Ni, L., *et al.* (2002) Functional profiling of the *Saccharomyces cerevisiae* genome. *Nature* **418**, 387–391.

Hegde, A.N. & Upadhya, S.C. (2007) The ubiquitin–proteasome pathway in health and disease of the nervous system. *Trends Neurosci.* **30**, 587–595.

Hershko, A. & Ciechanover, A. (1998) The ubiquitin system. *Annu. Rev. Biochem.* **67**, 425–479.

Hirokawa, T., Boon-Chieng, S. & Mitaku, S. (1998) SOSUI: classification and secondary structure prediction system for membrane proteins. *Bioinformatics* **14**, 378–379.

Ishiguro, A., Ideta, M., Mikoshiba, K., Chen, D.J. & Aruga, J. (2007) Zic2-dependent transcriptional regulation is mediated by DNA-dependent protein kinase, poly(ADP-ribose) polymerase and RNA helicase A. *J. Biol. Chem.* **282**, 9983–9995.

Jensen, K., Shiels, C. & Freemont, P.S. (2001) PML protein isoforms and the RBCC/TRIM motif. *Oncogene* **20**, 7223–7233.

Joazeiro, C.A. & Weissman, A.M. (2000) RING finger proteins: mediators of ubiquitin ligase activity. *Cell* **102**, 549–552.

Johnston, J.A. & Madura, K. (2004) Rings, chains and ladders: ubiquitin goes to work in the neuron. *Prog Neurobiol* **73**, 227–257.

Kostova, Z. & Wolf, D.H. (2003) For whom the bell tolls: protein quality control of the endoplasmic reticulum and the ubiquitin–proteasome connection. *EMBO J.* **22**, 2309–2317.

Lenk, U., Yu, H., Walter, J., Gelman, M.S., Hartmann, E., Kopito, R.R. & Sommer, T. (2002) A role for mammalian Ubc6 homologues in ER-associated protein degradation. *J. Cell Sci.* **115**, 3007–3014.

Lerner, M., Corcoran, M., Cepeda, D., Nielsen, M.L., Zubarev, R., Ponten, F., Uhlen, M., Hober, S., Grander, D. & Sangfelt, O. (2007) The RBCC gene RFP2 (Leu5) encodes a novel transmembrane E3 ubiquitin ligase involved in ERAD. *Mol. Biol. Cell* **18**, 1670–1682.

Mizugishi, K., Aruga, J., Nakata, K. & Mikoshiba, K. (2001) Molecular properties of Zic proteins as transcriptional regulators and their relationship to GLI proteins. *J. Biol. Chem.* **276**, 2180–2188.

Mizugishi, K., Hatayama, M., Tohmonda, T., Ogawa, M., Inoue, T., Mikoshiba, K. & Aruga, J. (2004) Myogenic repressor I-mfa interferes with the function of Zic family proteins. *Biochem. Biophys. Res. Commun.* **320**, 233–240.

Moriyoshi, K., Iijima, K., Fujii, H., Ito, H., Cho, Y. & Nakanishi, S. (2004) Seven in absentia homolog 1A mediates ubiquitination and degradation of group 1 metabotropic glutamate receptors. *Proc. Natl. Acad. Sci. USA* **101**, 8614–8619.

Munoz-Alonso, M.J., Guillemain, G., Kassis, N., Girard, J., Burnol, A.F. & Leturque, A. (2000) A novel cytosolic dual specificity phosphatase, interacting with glucokinase, increases glucose phosphorylation rate. *J. Biol. Chem.* **275**, 32406–32412.

Nagai, T., Aruga, J., Minowa, O., Sugimoto, T., Ohno, Y., Noda, T. & Mikoshiba, K. (2000) Zic2 regulates the kinetics of neurulation. *Proc. Natl. Acad. Sci. USA* **97**, 1618–1623.

Nagai, T., Aruga, J., Takada, S., Gunther, T., Sporle, R., Schughart, K. & Mikoshiba, K. (1997) The expression of the mouse *Zic1*, *Zic2*, and *Zic3* gene suggests an essential role for *Zic* genes in body pattern formation. *Dev Biol.* **182**, 299–313.

Nakagawa, Y., Kaneko, T., Ogura, T., Suzuki, T., Torii, M., Kaibuchi, K., Arai, K., Nakamura, S. & Nakafuku, M. (1996) Roles of cell-autonomous mechanisms for differential expression of region-specific transcription factors in neuroepithelial cells. *Development* **122**, 2449–2464.

Pickart, C.M. (2001) Mechanisms underlying ubiquitination. *Annu. Rev. Biochem.* **70**, 503–533.

Ravid, T., Kreft, S.G. & Hochstrasser, M. (2006) Membrane and soluble substrates of the Doa10 ubiquitin ligase are degraded by distinct pathways. *EMBO J.* **25**, 533–543.

Reymond, A., Meroni, G., Fantozzi, A., Merla, G., Cairo, S., Luzi, L., Riganelli, D., Zanaria, E., Messali, S., Cainarca, S., Guffanti, A., Minucci, S., Pelicci, P.G. & Ballabio, A. (2001) The tripartite motif family identifies cell compartments. *EMBO J.* **20**, 2140–2151.

Rost, B., Fariselli, P. & Casadio, R. (1996) Topology prediction for helical transmembrane proteins at 86% accuracy. *Protein Sci.* **5**, 1704–1718.

Sommer, T. & Jentsch, S. (1993) A protein translocation defect linked to ubiquitin conjugation at the endoplasmic reticulum. *Nature* **365**, 176–179.

Strausberg, R.L., Feingold, E.A., Grouse, L.H., *et al.* (2002) Generation and initial analysis of more than 15 000 full-length human and mouse cDNA sequences. *Proc. Natl. Acad. Sci. USA* **99**, 16899–16903.

Swanson, R., Locher, M. & Hochstrasser, M. (2001) A conserved ubiquitin ligase of the nuclear envelope/endoplasmic reticulum that functions in both ER-associated and Matα2 repressor degradation. *Genes Dev.* **15**, 2660–2674.

Turner, D.L. & Weintraub, H. (1994) Expression of *achaete-scute homolog 3* in *Xenopus* embryos converts ectodermal cells to a neural fate. *Genes Dev.* **8**, 1434–1447.

Yao, I., Takagi, H., Ageta, H., *et al.* (2007) SCRAPPER-dependent ubiquitination of active zone protein RIM1 regulates synaptic vesicle release. *Cell* **130**, 943–957.

Younger, J.M., Chen, L., Ren, H.Y., Rosser, M.F., Turnbull, E.L., Fan, C.Y., Patterson, C. & Cyr, D.M. (2006) Sequential quality-control checkpoints triage misfolded cystic fibrosis transmembrane conductance regulator. *Cell* **126**, 571–582.

Received: 19 September 2007
Accepted: 10 January 2008

Available online at www.sciencedirect.com
ScienceDirect
Neuroscience Research xxx (2008) xxx–xxx
Neuroscience Research
www.elsevier.com/locate/neures

L347P PINK1 mutant that fails to bind to Hsp90/Cdc37 chaperones is rapidly degraded in a proteasome-dependent manner

Yasuhiro Moriwaki [a,b], Yeon-Jeong Kim [b], Yukari Ido [a], Hidemi Misawa [a], Koichiro Kawashima [a], Shogo Endo [c], Ryosuke Takahashi [b,d,*]

[a] *Department of Pharmacology, Kyoritsu University of Pharmacy, 1-5-30 Shibakoen, Minato-ku, Tokyo 105-8512, Japan*
[b] *Laboratory for Motor System Neurodegeneration, RIKEN Brain Science Institute, 2-1 Hiroswa, Wako-Shi, Saitama 351-0198, Japan*
[c] *Unit for Molecular Neurobiology of Learning and Memory, Initial Research Project, Okinawa Institute of Science and Technology, Uruma, Okinawa 904-2234, Japan*
[d] *Department of Neurology, Kyoto University Graduate School of Medicine, 54 Kawahara-cho, Shogoin, Sakyo-ku, Kyoto 606-8507, Japan*

Received 26 November 2007; accepted 15 January 2008

Abstract

Mutation of PTEN-induced kinase 1 (*PINK1*), which encodes a putative mitochondrial serine/threonine kinase, leads to PARK6, an autosomal recessive form of familial Parkinson's disease. Although the precise function(s) of PINK1 protein is unknown, the recessive inheritance of this form of Parkinson's disease suggests loss of PINK1 function is closely associated with its pathogenesis. Here we report that PINK1 forms a complex with the molecular chaperones Hsp90 and Cdc37/p50 within cells, which appears to enhance its stability. When cells were treated with an Hsp90 inhibitor (geldanamycin or novobiocin), levels of PINK1 were greatly diminished, reflecting its rapid degradation via ubiquitin-proteasome pathway. Similarly, the half-life of a pathogenic PINK1 mutant (L347P) that did not interact with Hsp90 or Cdc37/p50 was only 30 min, whereas that of wild-type PINK1 was 1 h. These results strongly suggest that Hsp90 and Cdc37 are binding partners of PINK1 which regulate its stability.

Keywords: Parkinson's disease; PINK1; Hsp90; Cdc37; Proteasome; Stability

1. Introduction

Parkinson's disease (PD) is the second most frequently occurring neurodegenerative disorder and is characterized by selective dopaminergic neural cell loss in the substantia nigra (Dauer and Przedborski, 2003). Most cases of PD are sporadic; in 5–10% of the PD patients, however, the cause is an inherited gene mutation. Moreover, the fact that the clinical characteristics of familial PD are similar to those of sporadic PD has lead to efforts to understand the pathogenic mechanisms induced by the related gene mutations. Several genes are now known to be causally associated with familial PD (Abou-Sleiman et al., 2006). Among them, mutations in the PTEN-induced putative kinase 1 gene (*PINK1*) have been shown to be associated with an autosomal recessive form of familial PD (Valente et al., 2004).

PINK1 was initially isolated from endometrial cancer cells overexpressing PTEN (Unoki and Nakamura, 2001), and the predicted primary sequence of PINK1 protein included an N-terminal mitochondrial-targeting signal along with a catalytic serine/threonine kinase domain. Although PINK1's mitochondrial localization and self-directed phosphorylation activity have already been characterized (Valente et al., 2004; Beilina et al., 2005; Silvestri et al., 2005; Nakajima et al., 2003), its relation to the pathogenesis of PD is poorly understood. However, evidence from several recent studies suggests that PINK1 has the ability to protect cells from stress-induced mitochondrial dysfunction and apoptosis (Valente et al., 2004; Petit et al., 2005; Deng et al., 2005; Park et al., 2006; Clark et al., 2006; Tang et al., 2006). In addition, Deng et al. (2005) recently showed that suppression of PINK1 expression reduces cell viability and significantly increases 1-methyl-4-phenylpyridinium (MPP^+)- and rotenone-induced cytotoxicity. Consistent with those findings, *PINK1*-null flies exhibit male sterility,

* Corresponding author at: Department of Neurology, Kyoto University Graduate School of Medicine, 54 Kawahara-cho, Shogoin, Sakyo-ku, Kyoto 606-8507, Japan. Tel.: +81 75 751 3770; fax: +81 75 761 9780.
E-mail address: ryosuket@kuhp.kyoto-u.ac.jp (R. Takahashi).

0168-0102/$ – see front matter
doi:10.1016/j.neures.2008.01.006